THE JOURNAL OF BIOLOGICAL CHEMISTRY VOL. 289, NO. 3, pp. 1213–1226, January 17, 2014

Brain-derived Neurotrophic Factor (BDNF)-induced Mitochondrial Motility Arrest and Presynaptic Docking Contribute to BDNF-enhanced Synaptic Transmission*◆

Received for publication, October 11, 2013, and in revised form, November 23, 2013 Published, JBC Papers in Press, December 3, 2013, DOI 10.1074/jbc.M113.526129

Bo Su (苏擘)[1], Yun-Song Ji (纪云松)[1], Xu-lu Sun (孙旭璐), Xiang-Hua Liu (刘祥华), and Zhe-Yu Chen (陈哲宇)[2]

From the Department of Neurobiology, Shandong Provincial Key Laboratory of Mental Disorders, School of Medicine, Shandong University, Jinan, Shandong 250012, China

Background: Appropriate mitochondrial transport and localization are highly associated with neuronal activities.
Results: BDNF induces mitochondrial motility arrest via Miro1 binding with Ca^{2+}, which facilitates BDNF-enhanced neurotransmitter release.
Conclusion: BDNF-regulated mitochondrial motility is essential for BDNF-enhanced synaptic transmission.
Significance: These results provide novel insights into the mechanistic link between BDNF-dependent mitochondrial motility and BDNF-mediated synaptic transmission.

Appropriate mitochondrial transport and distribution are essential for neurons because of the high energy and Ca^{2+} buffering requirements at synapses. Brain-derived neurotrophic factor (BDNF) plays an essential role in regulating synaptic transmission and plasticity. However, whether and how BDNF can regulate mitochondrial transport and distribution are still unclear. Here, we find that in cultured hippocampal neurons, application of BDNF for 15 min decreased the percentage of moving mitochondria in axons, a process dependent on the activation of the TrkB receptor and its downstream PI3K and phospholipase-Cγ signaling pathways. Moreover, the BDNF-induced mitochondrial stopping requires the activation of transient receptor potential canonical 3 and 6 (TRPC3 and TRPC6) channels and elevated intracellular Ca^{2+} levels. The Ca^{2+} sensor Miro1 plays an important role in this process. Finally, the BDNF-induced mitochondrial stopping leads to the accumulation of more mitochondria at presynaptic sites. Mutant Miro1 lacking the ability to bind Ca^{2+} prevents BDNF-induced mitochondrial presynaptic accumulation and synaptic transmission, suggesting that Miro1-mediated mitochondrial motility is involved in BDNF-induced mitochondrial presynaptic docking and neurotransmission. Together, these data suggest that mitochondrial transport and distribution play essential roles in BDNF-mediated synaptic transmission.

Mitochondria are important organelles with multiple functions, including ATP production, the maintenance of intracellular Ca^{2+} homeostasis, and the regulation of apoptosis. In neurons, proper mitochondrial trafficking and distribution along neurites are involved in synaptic plasticity modulation such as presynaptically neurotransmitter release, postsynaptically membrane trafficking of ion channels, and dendritic spine maturation (1, 2).

Recent work has begun to reveal the mechanisms underlying mitochondrial motility. *In vivo* and *in vitro* studies have identified several kinesin family members, including KIF5A/B/C, KIF1Bα, and KLP6, that are involved in mitochondrial anterograde transport (3–7). In addition to the motor proteins, intracellular signaling pathways that regulate mitochondrial movement have also been investigated. It has been reported that nerve growth factor (NGF) affects mitochondrial motility by its downstream phosphoinositide 3-kinase (PI3K) signaling pathway (8). Edelman and co-workers (9, 10) have demonstrated that Akt-glycogen synthase kinase 3β (GSK3β) is associated with axonal mitochondrial transport stimulated by serotonin and dopamine. Calcium has been demonstrated to be one of the critical factors that regulate mitochondrial transport (11–13). Recently, a complex composed of KIF5, Milton/TRAK, and Miro1 was reported to mediate mitochondrial transport along microtubules; Miro1 as the Ca^{2+} sensor could regulate mitochondrial anterograde and retrograde movement in both axons and dendrites (13–16).

BDNF[3] is broadly expressed in the central nervous system and plays critical roles in regulating neuronal survival, development, and synaptic plasticity. The actions of BDNF are dictated by two classes of receptors on the cell surface, TrkB and p75. Upon activation of TrkB receptors, several signaling pathways

* This work was supported by National 973 Basic Research Program of China Grant 2012CB911000, National Natural Science Foundation of China Grants 31130026 and 31100968, State Program of National Natural Science Foundation of China for Innovative Research Group Grant 81321061, China Postdoctoral Science Foundation Grants 20110491590 and 2012T50609, Specialized Research Fund for the Doctoral Program of Higher Education 20100131120052, and the Independent Innovation Foundation of Shandong University.
◆ This article was selected as a Paper of the Week.
[1] Both authors contributed equally to this work.
[2] To whom correspondence should be addressed: Dept. of Neurobiology, School of Medicine, Shandong University, No. 44 Wenhua Xi Rd., Jinan, Shandong 250012, China. Tel.: 86-531-88382336; Fax: 86-531-88382329; E-mail: zheyuchen@sdu.edu.cn.

[3] The abbreviations used are: BDNF, brain-derived neurotrophic factor; DIV, days *in vitro*; TrkB, tropomyosin-related kinase B; TRPC, transient receptor potential cation channels; DN, dominant negative; BAPTA-AM, 1,2-bis(2-aminophenoxy)ethane-*N*,*N*,*N*′,*N*′-tetraacetic acid tetrakis(acetoxymethyl ester); PLC, phospholipase-C; Xest C, xestospongin C; OAG, 1-oleoyl-2-acetyl-*sn*-glycerol; DAG, diacylglycerol; IP_3, inositol 1,4,5-triphosphate; IP_3R, IP_3 receptor; 2APB, 2-aminoethoxydiphenyl borate.

are activated, including MAPK, PI3K, and phospholipase-Cγ (17). It has been reported that in addition to regulating synaptic plasticity, BDNF can stimulate brain mitochondrial metabolism by increasing the efficiency of respiratory coupling and ATP synthesis (18). However, the mechanism by which BDNF regulates mitochondrial function is still unclear. In particular, it remains unknown whether BDNF can regulate mitochondrial transport and distribution in neurons.

In this study, we investigated the effects of BDNF on mitochondrial motility in primary hippocampal neurons. We report that BDNF could induce more mitochondrial docking at presynaptic sites, an effect mediated by the elevation of intracellular Ca^{2+} through PI3K and PLCγ signaling pathways and transient receptor potential canonical (TRPC) channels in a Miro1-dependent manner. More importantly, BDNF-enhanced synaptic transmission is prevented by mutant Miro1 lacking the ability to bind Ca^{2+}, indicating an important role for presynaptically accumulated mitochondria on neurotransmission.

EXPERIMENTAL PROCEDURES

Reagents and Antibodies—Human recombinant BDNF was purchased from PeproTech (Rocky Hill, NJ). BAPTA-AM and K-252a were obtained from Calbiochem. Other inhibitors and activators were obtained from Sigma. Antibodies were purchased as follows: mouse anti-Miro1 antibody from Abnova (Taipei, Taiwan); rabbit anti-Kinesin 5A+B+C antibody from Abcam (Cambridge, MA); rabbit anti-VDAC antibody from Cell Signaling (Danvers, MA); mouse anti-GAPDH antibody from Upstate (Billerica, MA); rabbit anti-TrkB antibody from Millipore (Billerica, MA); mouse monoclonal anti-SV2 antibody from the Developmental Studies Hybridoma Bank (Iowa City, IA); horseradish peroxidase-conjugated goat anti-mouse or -rabbit IgG antibodies used for Western blot from Calbiochem; and Alexa Fluor 488- or 594- or Cy5-conjugated goat anti-mouse or rabbit IgG heavy and light chains (H+L) used for immunofluorescent staining from Invitrogen. Restriction enzymes were purchased from Fermentas (Hanover, MD). Fluo4-AM, JC-1, FM 1-43 AM, trypsin, and cell culture reagents were purchased from Invitrogen. The ATP assay kit and mitochondrial isolation kit were purchased from Beyotime Institute of Biotechnology (Haimen, Jiangsu, China). All other reagents were from Sigma unless otherwise noted.

Plasmids Construction and siRNA—The pDsRed2-mito, which encodes mitochondrial targeted DsRed fluorescent protein, was purchased from Clontech. The coding region of rat Miro1 was amplified from rat cDNA and subcloned into pcDNA 3.1-flag (Invitrogen) and pEGFP-C2 (Clontech) expression vectors. The EF domain mutant rat Miro1 (E221K and E341K) construct was generated by means of a three-step PCR. Rab5 was constructed from rat cDNA and inserted into pEGFP-N1 (Clontech). The target sequences of TRPC3, TRPC5, and TRPC6 siRNAs were from previous studies (19–21), as follows: TRPC3 5′-GGCTGCGCATTGCCATAAA-3′, TRPC5 5′-CACTCTTCGCGATATCGAA-3′, and TRPC6 5′-GAACGGCCTCATGATTATT-3′. All the siRNAs were subcloned into the pSuper-mRFP vector (OligoEngine, Seattle) according to the manufacturer's protocol, and the efficiency was confirmed by real time PCR. Dominant-negative constructs of TRPC3, TRPC5, and TRPC6 were kindly provided by Yizheng Wang (Neurobiology Institute, Shanghai, China). All of the constructs were confirmed by DNA sequencing to exclude potential mutations introduced by PCR.

Neuronal Cultures and Transfection—Cultures of hippocampal neurons were prepared from timed Sprague-Dawley rat brains as described previously (22). In brief, hippocampi dissected from embryonic day 18 rats were placed into ice-cold Hanks' balanced saline solution, digested with 0.05% trypsin/EDTA at 37 °C for 10 min, and triturated in DMEM/F-12 medium containing 10% fetal bovine serum. Neurons were seeded onto coverslips coated with 0.1 mg/ml poly-D-lysine in 6-well plates at a density of $3–8 \times 10^5$ and then cultured in Neurobasal medium containing 2% B27 supplement and 0.5 mM L-glutamine. Neurons were cultured in an incubator at 37 °C with 5% CO_2 at 95% humidity for 12–14 days before treating with 50 ng/ml BDNF or other experiments, and the medium was half-changed every 3–4 days. The concentration of 50 ng/ml is a saturated dose for neurons and has been customarily used for the studies of the effects of BDNF on neuronal dendritic growth and synaptic activities (23, 24). We used this concentration for all experiments. The neurons were transfected with Lipofectamine 2000 (Invitrogen) following the manufacturer's instructions at 8–10 days *in vitro* (DIV) and used 2–4 days after transfection.

Mitochondrial Isolation and Western Blot—Mitochondria were isolated from cultured neurons at 12–14 DIV with the mitochondrial isolation kit from Beyotime Co. following the manufacturer's instructions. Briefly, cultured neurons in 10-cm dishes were starved in Neurobasal medium without B27 for 8 h and then treated with BDNF (50 ng/ml) for 15 min at 37 °C. After that, neurons were harvested in mitochondrial isolation buffer with PMSF and transferred to a grinder for crushing until the solution became homogeneous. The mitochondria were isolated by differential centrifugation at $600 \times g$ and $3000 \times g$ for 10 min at 4 °C, respectively, and stored in mitochondrial lysis buffer. For Western blotting, the mitochondrial proteins were boiled with 4× sample buffer for 5 min and separated by SDS-PAGE. After transfer to a polyvinylidene difluoride (PVDF) membrane (Bio-Rad), the proteins were probed with the noted primary antibodies and the corresponding HRP-conjugated secondary antibodies. Finally, the Western blot signals were detected using the ECL detection kit (Millipore) and quantified with Quantity One (Bio-Rad).

Real Time PCR—Quantitative real time PCR was used to determine the efficiency of knockdown of TRPC3, TRPC5, and TRPC6 by siRNA. Because of the low transfection efficiency in primary hippocampal neurons, the rat-derived PC12 cell line was used to examine the knockdown efficiency. First, PC12 cells were transfected with TRPC3, TPRC5, or TRPC6 siRNA. Two days after transfection, total mRNA was isolated from cells using the Ultrapure RNA kit (CoWin Biotech, Beijing, China). The RNA from each sample was reverse-transcribed into cDNA using ReverTra Ace qPCR RT kit (Toyobo, Osaka, Japan) with oligo(dT) and random primers according to the manufacturer's instructions. Quantitative real time PCR was performed using FastStart Universal SYBR Green Master (Roche Applied Science). The primer sequences are as follows: TRPC: forward

primer, 5′-CCACATGCAGTGAGACTTTGACTC-3′, and reverse primer, 5′-AGGCCAACCTTGGGATCATTT-3′; TRPC5 forward primer, 5′-AAGTTTCGAATTTGAGGAGCAGATG-3′, and reverse primer, 5′-AATCTCTGATGGCATCGCACA-3′; TRPC6 forward primer, 5′-GCCTCATGATTATTTCTGCAAGTGTAC-3′, and reverse primer, 5′-TGAACTCTTTCTCAATGTTGGCAA-3′; and β-actin forward primer, 5′-tccatcatgaagtgtgacgt-3′, and reverse primer, 5′-gagcaatgatcttgatcttcat-3′. Each sample was analyzed in triplicate, and the mRNA levels were normalized to β-actin mRNA levels using the $2^{-\Delta\Delta}C_t$ method.

Immunofluorescence Staining and Image Processing—To analyze the localization of mitochondria in neuronal synaptic sites, neurons at 8–10 DIV were transfected with mitoDsRed2 to label mitochondria. Two to 4 days after transfection, neurons were fixed with 4% paraformaldehyde, permeabilized with 0.4% Triton X-100, and then blocked with 10% goat serum. Presynaptic sites were labeled with SV2 antibody (recognizing synaptic vesicles) followed by Alexa Fluor 488-conjugated or Cy5-conjugated goat anti-mouse IgG. The dendrites and axons can be clearly distinguished; mitoDsRed2-labeled axons were shown as long thin processes, whereas the dendrites were far shorter and thicker and had a different branching morphology. Axonal mitochondrial localization at presynaptic sites was measured as follows: circular regions of interest with a radius of 1 μm from the SV2 puncta were placed around each identified puncta, and mitochondria occupying at least half of the radius of a region of interest in the same axon were considered to be colocalized with SV2 puncta. Fluorescence images were acquired with a Nikon Eclipse TE 2000-U microscope. All of the images were collected using a 60× oil immersion objective lens and processed with MetaMorph software (Universal Imaging Corp., West Chester, PA). All the images were acquired under the same conditions. To avoid errors due to subjective intention, an investigator blind to the experimental conditions analyzed the images using ImageJ.

To examine the surface expression of TrkB in neurons expressing Miro1 and Miro1^{KK}, hippocampal neurons were cotransfected with pEGFP-N1 and pcDNA3.1 FLAG-Miro1/Miro1^{KK} at a ratio of 1:5. We confirmed that neurons expressing GFP also express Miro1 or Miro1^{KK} (data not shown). Two days after transfection, the neurons were fixed with 4% paraformaldehyde in PBS for 15 min. Then the neurons were rinsed three times in PBS and blocked in 10% goat serum for 1 h at room temperature. Surface TrkB was stained using rabbit anti-TrkB antibody (Millipore, 1:300), which recognizes the extracellular domain of TrkB, in blocking buffer for 1 h at room temperature. Surface TrkB was subsequently detected by incubation with Alexa Fluor 594-conjugated goat anti-rabbit IgG. Acquired images were analyzed using ImageJ software.

Live Imaging—Neurons were cultured on 35-mm glass bottom culture dishes at a density of 5×10^5/dish (MatTek, Ashland, MA). For image acquisition, dishes were placed in a live-imaging station mounted on a Nikon Eclipse TE 2000-U microscope in an atmosphere of 37 °C and 5% CO_2, and all the photos were collected using a 40× oil immersion objective lens and processed by MetaMorph software. Live images were captured every 3 s for 5 min before and after BDNF or other inhibitors were applied. Analyses were performed on 150 μm of axon at least 50 μm away from the cell body. Kymographs were generated with ImageJ software and show the axon along the *x* axis and time across the *y* axis. The length of the kymographs is 5 min, and time increases down the formed photos. Mitochondrial motility was assessed by counting the percentage of moving mitochondria during an imaging period (5 min unless stated otherwise). Mitochondrial velocity was measured using the MTrackJ plugin of ImageJ.

FM 1-43 Staining—FM 1-43 staining was carried out as described previously with a few modifications (25–27). For labeling active presynaptic boutons, the neurons were stimulated by superfusing with the hyperkalemic solution (31.5 mM NaCl, 90 mM KCl, 2 mM $CaCl_2$, 2 mM $MgCl_2$, 25 mM HEPES, 30 mM glucose) containing FM 1-43 (5 μM) for 45 s. During the loading period, the dye was rapidly taken up into presynaptic terminals as the released vesicles underwent endocytosis. The extracellular solution was then switched to normal saline solution (119 mM NaCl, 2.5 mM KCl, 2 mM $CaCl_2$, 2 mM $MgCl_2$, 25 mM HEPES, 30 mM glucose). ADVASEP-7 (1 mM) was introduced for 60 s at 1 and 6 min for enhanced removal of the dye from the external medium. A schematic of the procedure is provided in Fig. 8*A*. An image was then taken to record the loading of FM 1-43 in the synaptic boutons (I). The cultures were then exposed to multiple 15-s applications of hyperkalemic bath solution (without FM 1-43 dye) to evoke repeated cycles of exocytosis, which facilitate the release of the dye trapped in the active vesicles. After 30 min of repeated cycles of exocytosis, another image (II) was taken. The difference in the number of FM 1-43-labeled boutons in the axonal regions between I and II was calculated to indicate the number of active presynaptic boutons.

To study BDNF-induced neurotransmitter release, after loading and unloading of the FM 1-43 dye, the cultures were exposed to human recombinant BDNF (50 ng/ml) for 15 min, and the procedure of staining and destaining was then repeated. A schematic of the procedure is provided in Fig. 8*A*. To measure the plasticity changes in presynaptic terminals stimulated by BDNF, we compared the differences in changes of FM 1-43 fluorescence intensity along the GFP-labeled axons before (I and II) and after treatment with BDNF (III and IV). To block possible recurrent excitation and induction of active-dependent plasticity, 40 μM D-2-amino-5-phosphonovalerate (NMDA receptor antagonist) and 20 μM 6-cyano-7-nitroquinoxaline-2,3-dione (the non-NMDA receptor antagonist) were included in the hyperkalemic solution. All images were taken using a Nikon Eclipse TE 2000-U microscope with 40× oil immersion objective lens and analyzed with ImageJ software. The individual puncta were identified based on a fluorescence intensity that exceeded a threshold set above background and a diameter between 0.5 and 3 μm. To avoid objective errors, all images were subjected to exactly the same acquisition and analysis conditions. The investigator was blind to the experimental conditions.

To study the effects of Miro1 on BDNF-induced synaptic function, we transfected neurons with pEGFP-N1 and pcDNA3.1 FLAG-WT Miro1 or pCDNA3.1-Miro1^{KK} in the proportion of 1:5 at 9 DIV, such that neurons expressing GFP

also expressed WT Miro1 or Miro1^{KK}. The active synaptic boutons and the BDNF-induced neurotransmitter release were examined as described above at 12–14 DIV.

Mitochondrial Membrane Potential Assay—Mitochondrial membrane potential was measured in live neurons with the use of the fluorescent probe JC-1. With higher mitochondrial membrane potentials, JC-1 forms red fluorescent aggregates in mitochondria, with a broad excitation spectrum and a maximum emission at 590 nm. However, at lower membrane potentials, JC-1 exists as fluorescent green monomers with emission at 527 nm when excited at 490 nm. Neurons at 12–14 DIV were loaded with 2 μg/ml JC-1, incubated at 37 °C for 30 min, then washed twice with medium, and imaged in conditioned culture medium. JC-1 fluorescent signals in live neurons were collected using a Carl Zeiss LSM-780 confocal microscope with a Plan Apochromat 63× oil immersion objective lens (NA 1.40) (Microstructural Platform of Shandong University). JC-1 was excited at 488 nm (green) and 561 nm (red), and its corresponding fluorescent emission was collected using bandpass (BP 490–550 nm) and long path emission filters (LP 590 nm) for monomer and aggregate signals, respectively. Three to four fields from each culture dish were selected and imaged. For mitochondrial membrane potential measurement, the JC-1 fluorescent intensity, defined as the red to green ratio, was calculated using ImageJ.

ATP Production Assay—The neuronal ATP level was measured using the ATP assay kit from Beyotime Co. Briefly, the lysate of cultured neurons was collected and centrifuged at 10,000 × *g* for 10 min at 4 °C, and then the ATP level in the supernatant was examined by mixing the supernatant with luciferase reagent. The emitted light was measured using a microplate luminometer. The protein level was determined using a BCA protein assay kit (Thermo Scientific, Rockford, IL). The ATP level was normalized to the protein concentration of each sample.

Intracellular Ca^{2+} Measurement—The changes of intracellular calcium concentration were examined by Fluo4-AM staining. Neurons were incubated with 2 μM Fluo4-AM in Neurobasal medium for 30 min at 37 °C, followed by incubation for another 30 min after rinsing with Hanks' balanced saline solution. Ca^{2+} imaging was performed using a spinning disk confocal microscope (Cell Observer SD) with a 40× oil immersion objective (Microstructural Platform of Shandong University). Cells were excited with a laser at 488 nm, and the intensity of the fluorescence was collected at 525 nm as the Fluo4-AM signal. The images were collected before and after BDNF treatment, and the fluorescent intensity was analyzed with ImageJ. To measure the calcium in the axonal terminals, neurons were transfected with red fluorescent protein vector to label the neurites, and the axons and dendrites could be distinguished by their morphology. The axon terminals could be found along the axon extending from the soma, and the Fluo4-AM-labeled axonal tips were analyzed before and after BDNF application.

Statistical Analysis—The results of more than three independent experiments were compiled, and they were analyzed using Student's *t* test or one-way analysis of variance followed by post hoc tests. Data are shown as the mean ± S.E. Statistical significance was determined with *, $p < 0.05$; **, $p < 0.01$.

RESULTS

BDNF Treatment Induces Reduced Mitochondrial Motility in Axons—To measure axonal mitochondrial movement, we carried out live cell microscopy of rat neurons expressing mitoDsRed2 (labeling mitochondria without affecting their movement). Cultured hippocampal neurons at 12–14 DIV were bath-incubated with 50 ng/ml BDNF for 15 min, and mitochondrial motility in axons was examined. The dendrites and axons can be distinguished; the mitoDsRed2-labeled axons were visible as long thin processes, although the dendrites were far shorter and thicker and had a different branching morphology. Kymographs were created with the axon along the *x* axis and the time along the *y* axis. Stationary and moving mitochondria can be seen as straight lines and diagonal lines, respectively. As shown in Fig. 1, *A–C*, BDNF treatment significantly reduced axonal mitochondrial motility for both anterograde and retrograde movement. At basal status, the percentage of moving mitochondria in axons was ~13.3% for anterograde and 12.9% for retrograde over a 5-min period, similar to a previous report (13). However, BDNF treatment caused a significant decrease in the percentage of mobile mitochondria in axons for both directions (Fig. 1, *A–C*). Although the percentage of moving mitochondria was decreased, the velocity of the moving mitochondria was not affected by BDNF treatment (Fig. 1*D*). Thus, BDNF treatment increased the fraction of mitochondria in the stationary phase rather than altering the speed of moving mitochondria. To determine whether BDNF could affect the movement of organelles other than mitochondria, we also investigated the effect of BDNF on the motility of endosomes, which were labeled by GFP-tagged Rab5. No changes in the percentage of moving endosomes were observed upon BDNF treatment (Fig. 1, *E–G*), indicating that the effect of BDNF on mitochondrial motility is specific.

Because it has been demonstrated that BDNF can increase mitochondrial oxidative coupling and the efficiency of the ATP synthesis (18, 28), we further investigated whether BDNF-induced mitochondrial stopping was associated with mitochondrial membrane potential and ATP production. Mitochondrial membrane potential was examined with JC-1 staining. As shown in Fig. 2, *A* and *B*, no significant changes were observed after BDNF treatment for 15 min. However, extending the BDNF treatment to 24 and 72 h significantly increased the mitochondrial membrane potential. Creatine has been reported to stimulate mitochondrial respiration and membrane potential (2, 29). The neurons were treated with creatine for 18 h as a positive control (Fig. 2, *A* and *B*). ATP production was not affected by 15 min and 24 h of BDNF treatment, but lengthening the BDNF treatment to 72 h resulted in a slight but significant increase in ATP production (Fig. 2*C*). Thus, the above results suggest that BDNF-induced decreased mitochondrial motility precedes increases in mitochondrial functions such as mitochondrial membrane potential and ATP production.

Activation of PI3K and PLCγ Signaling Pathways Is Required for BDNF-induced Mitochondrial Stopping—Because BDNF treatment induced more mitochondria into the stationary pool, we next investigated the mechanisms underlying this phenomenon. We found that K252a, a widely used inhibitor of Trk

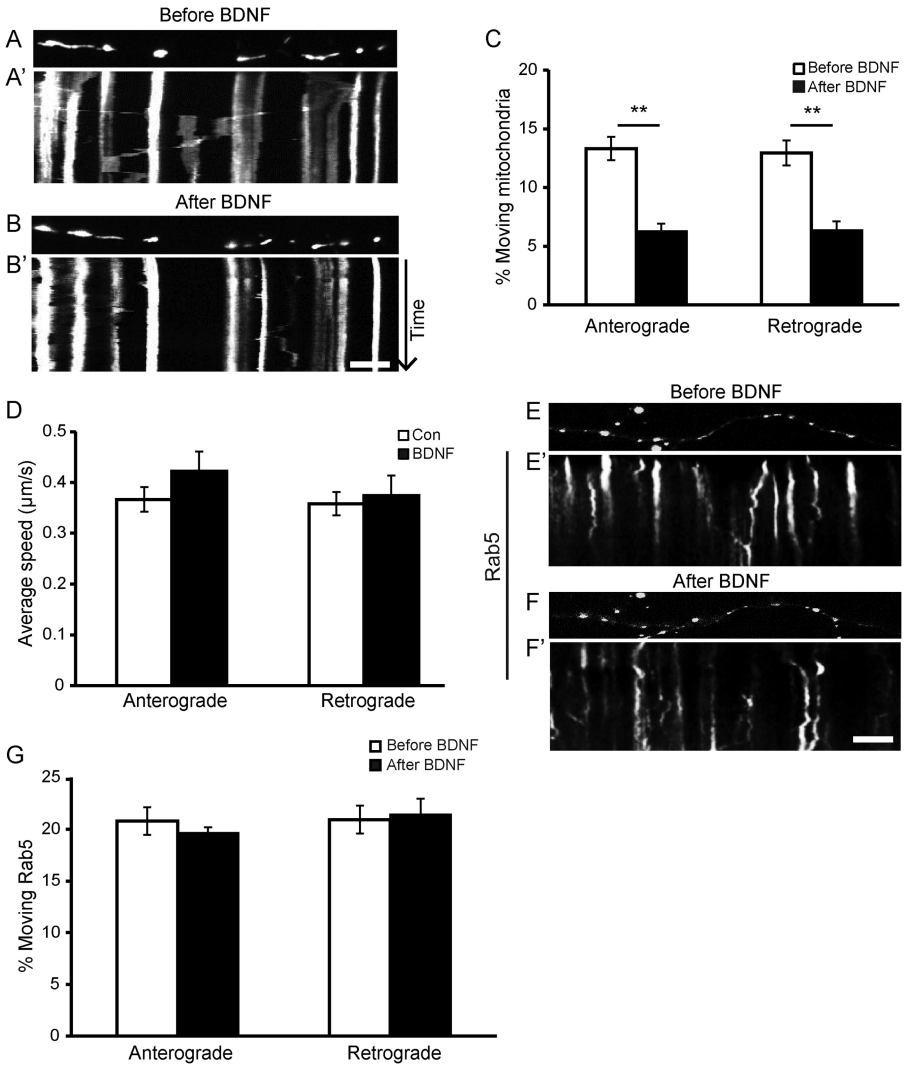

FIGURE 1. **BDNF induces more mitochondria into the stationary pool without affecting other organelles.** *A* and *B,* representative static images of mitochondria in neurites before (*A*) and after (*B*) BDNF treatment. *A′* and *B′,* representative kymographs showing decreased mitochondrial movement in neurites upon BDNF treatment (*B′*) compared with pretreatment (*A′*). *Scale bar,* 10 μm; height, 5 min. *C,* quantification of the percentages of anterograde- and retrograde-moving mitochondria in axons before and after BDNF treatment ($n = 442$ mitochondria from 19 axons and six independent experiments). *D,* BDNF treatment for 15 min had no effect on the velocity of the moving mitochondria ($n = 198$ mitochondria from 23 axons and at least four independent experiments). *E* and *F,* representative static images of Rab5 puncta before (*E*) and after (*F*) BDNF treatment. *E′* and *F′,* representative kymographs showing that the motility of Rab5-labeled endosomes was not affected by BDNF. Quantification data are shown in *G* ($n = 297$ Rab5 puncta from eight axons and three separate transfections). *Scale bar,* 10 μm; height, 5 min. Values are shown as the mean $\pm$ S.E., **, $p < 0.01$, Student's *t* test.

kinases, could completely block BDNF-induced mitochondrial stopping regardless of the movement direction, although the p75 inhibitor tat-PEP5 had no effect (Fig. 3*A*; the retrograde-moving mitochondria result is similar to anterograde-moving mitochondria and is not shown), indicating that the effect of BDNF on mitochondrial movement relies on TrkB kinase activity. Next, we used pharmacological inhibitors to investigate which signaling pathway downstream of TrkB activation was involved. A specific PLCγ inhibitor, U73122, abolished BDNF-induced mitochondrial stopping, whereas its inactive derivative U73343 had no effect (Fig. 3*B*). Pretreatment with the PI3K inhibitor LY294002 also abolished BDNF's effects on mitochondrial motility, whereas inactivating the MAPK with U0126 had no effect (Fig. 3*B*). These results suggest that activation of the PI3K and PLCγ signaling pathways is required for BDNF-induced mitochondrial stopping. A direct downstream effector of PLCγ is inositol 1,4,5-triphosphate (IP_3), which induces internal Ca^{2+} release by activating the IP3 receptor (IP_3R). Blocking IP_3R with xestospongin C or 2APB abolished BDNF-induced mitochondrial stopping (Fig. 3*B*). Another downstream effector of PLCγ is diacylglycerol (DAG), which then activates protein kinase C. The membrane-permeable DAG analog 1-oleoyl-2-acetyl-*sn*-glycerol (OAG) could not induce mitochondrial motility arrest, but when OAG was applied together with BDNF, a reduced percentage of moving mitochondria was observed, suggesting that DAG is not involved in BDNF-induced mitochondrial motility arrest (Fig. 3*B*). As observed in neurons pretreated with K252a, both anterograde and retrograde movements were blocked by inhibitors of PI3K, PLCγ, and IP_3R. The figures show only the results for anterograde-moving mitochondria. Thus, the results suggest that BDNF-induced mitochondrial stopping depends on PI3K and PLCγ-IP_3R activation but not on the PLCγ-DAG signaling pathway.

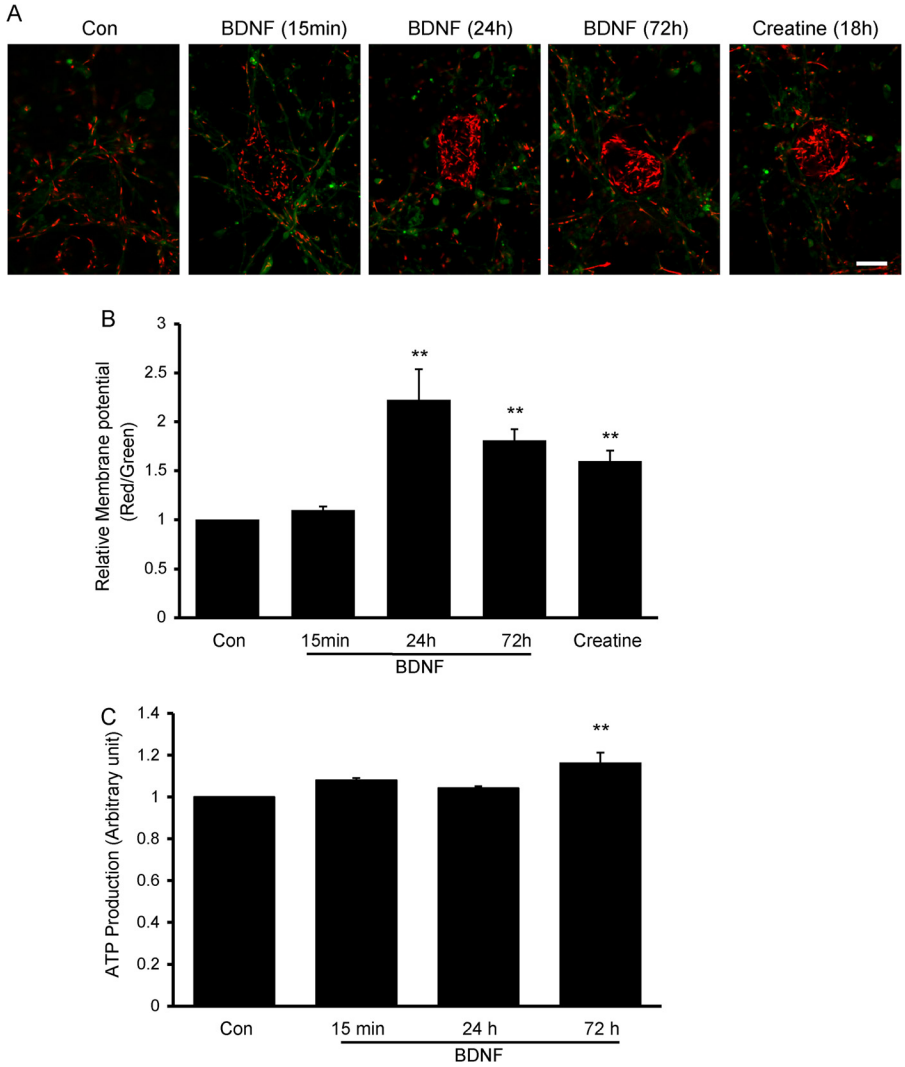

FIGURE 2. **Transient BDNF treatment has no effect on mitochondrial membrane potential or ATP production.** *A* and *B,* representative images of JC-1 staining of control (*Con*) neurons and neurons treated with BDNF or creatine (*A*). *Scale bar,* 20 μm. Mitochondrial membrane potential was not changed upon BDNF treatment for 15 min, but it increased significantly after BDNF treatment for 72 h. Creatine treatment for 18 h was used as a positive control (*B*). *C,* no changes in ATP production were observed after transient BDNF treatment, but ATP production increased significantly after BDNF treatment for 72 h. Values are shown as the mean ± S.E., **, $p < 0.01$, Student's *t* test.

Elevation of Intracellular Ca^{2+} Is Necessary for BDNF-induced Mitochondrial Stopping—It has been known that BDNF induces elevation of intracellular Ca^{2+} (19, 30), and Ca^{2+} has been reported to be an important regulator of mitochondrial movement (13, 16). We hypothesize that Ca^{2+} plays an important role in BDNF-regulated mitochondrial motility. Indeed, Fluo4-AM imaging revealed that BDNF induces significant elevation of intracellular Ca^{2+}, which reached high levels by 15 min and could remain at this level even after 30 min (Fig. 4*A*). The increased intracellular Ca^{2+} concentration could be suppressed by pretreatment with K252a, U73122, LY294002, or xestospongin C (Xest C) (TrkB, PLCγ, PI3K, and IP_3R inhibitors, respectively) (Fig. 4*B*), which is consistent with our previous result that these inhibitors could block the effect of BDNF on mitochondrial motility. The above result also suggests that IP_3R-regulated Ca^{2+} release from the internal store is required for BDNF-induced intracellular Ca^{2+} elevation. The membrane-permeable Ca^{2+} buffer BAPTA-AM and the extracellular Ca^{2+} depletion reagent EGTA also blocked BDNF-induced intracellular Ca^{2+} elevation (Fig. 4*B*), suggesting Ca^{2+} influx is required for BDNF-induced intracellular Ca^{2+} elevation. Therefore, BDNF-induced elevation of intracellular Ca^{2+} depends on both IP_3R-mediated intracellular Ca^{2+} release from internal stores and extracellular Ca^{2+} influx. Next, we investigated whether the intracellular Ca^{2+} indeed mediates the BDNF-induced stopping of mitochondria and which Ca^{2+} channel is involved in this process. Preincubation with BAPTA-AM (2 μM) or EGTA (2 mM), which blocked the BDNF-induced intracellular Ca^{2+} elevation, abolished the effect of BDNF on mitochondrial mobility in both directions (Fig. 4*C*, retrograde movement not shown). Therefore, the elevated Ca^{2+} is essential for the reduction in mitochondrial motility induced by BDNF. Pretreatment with nifedipine or ω-conotoxin MVIIC, which are inhibitors of L- and P/Q-type voltage-dependent Ca^{2+} channels, respectively, had no effects on BDNF-induced mitochondrial stopping. Applying a higher concentration of ryanodine (100 μM) to block ryanodine-sensitive internal Ca^{2+} channels also showed no effect on BDNF-

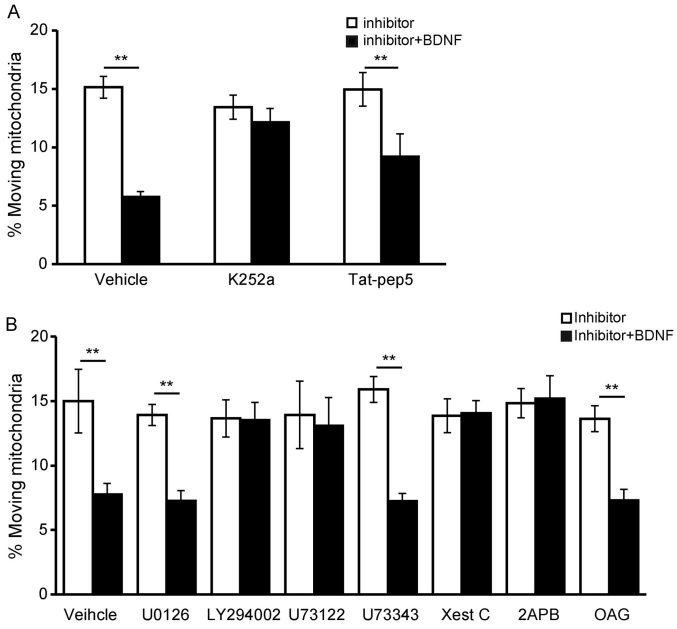

FIGURE 3. **TrkB, PLCγ, and PI3K are required for BDNF-induced mitochondrial stopping.** *A,* TrkB kinase activity is required for BDNF-induced mitochondrial stopping. The tyrosine kinase inhibitor K252a prevented BDNF-induced mitochondrial motility arrest, but the p75 signaling inhibitor Tat-PEP5 had no effect (control, $n = 247$ mitochondria from nine axons; K252a, $n = 185$ mitochondria from eight axons; Tat-PEP5, $n = 225$ mitochondria from nine axons). Quantification of anterograde-moving mitochondria is shown. *B,* neurons were pretreated with U0126 (MAPK inhibitor), LY294002 (PI3K inhibitor), U73122 (PLCγ inhibitor), U73343 (analog of U73122), xestospongin C (Xest C, IP3 receptor inhibitor), 2APB (IP_3 receptor inhibitor), or the diacylglycerol analog OAG and then exposed to BDNF for 15 min. The percentage of moving mitochondria in axons was measured (control, $n = 129$ mitochondria from eight axons; U0126, $n = 207$ mitochondria from nine axons; LY294002, $n = 208$ mitochondria from nine axons; U73122, $n = 203$ mitochondria from eight axons; U73343, $n = 142$ mitochondria from eight axons; Xest C, $n = 159$ mitochondria from nine axons; 2APB, $n = 115$ mitochondria from eight axons; OAG, $n = 254$ mitochondria from 10 axons). Quantification of anterograde-moving mitochondria is shown. Values are shown as the mean ± S.E. from four independent experiments, **, $p < 0.01$, Student's *t* test.

induced mitochondrial stopping (Fig. 4*C*). Thus, voltage-dependent Ca^{2+} channels and internal ryanodine channels are unlikely to contribute to BDNF-induced mitochondrial stopping.

Multiple findings have demonstrated that TRPC channels are Ca^{2+}-permeant channels activated by BDNF (19, 30, 31); therefore, we next investigated whether they are involved in BDNF-evoked stopping of mitochondria. When primary hippocampal neurons were pretreated with SKF-96365 (5 μM), a known nonspecific inhibitor of transient receptor potential channels, BDNF-induced mitochondrial stopping in both directions was completely abolished (Fig. 5, *A–E*, quantification of anterograde-moving mitochondria is shown), suggesting that TRPC channels participate in BDNF-induced mitochondrial stopping. Among the TRPC channels, TRPC3, TRPC5, and TRPC6 have been widely studied in neuronal systems (19, 30, 32–34). We next examined which TRPC channel contributed to the BDNF-induced mitochondrial stopping. TRPC3, TRPC5, or TRPC6 expression was knocked down by specific short interfering RNAs (siRNAs), and the knockdown efficiency was examined in PC12 cells by real time PCR (Fig. 5*F*). The effect of TPRC3, -5, or -6 on BDNF-regulated mitochondrial motility was then investigated. Introducing either TRPC3 or TRPC6 siRNAs in neurons abolished BDNF's effect on mitochondrial motility, but TRPC5 siRNA had no effect (Fig. 5*G*). To exclude off-target effects of the siRNAs, dominant-negative (DN) constructs of TRPC3, TRPC5, or TRPC6 labeled with green fluorescent protein (GFP) were transfected into hippocampal neurons. Transfection of DN-TRPC3 or DN-TRPC6, but not DN-TRPC5, abolished the effect of BDNF on mitochondrial motility (Fig. 5*G*), further confirming that TRPC3 and TRPC6 are essential in BDNF-induced mitochondrial stopping. Furthermore, BDNF-induced elevation of intracellular Ca^{2+} was also blocked in neurons with TRPC3 or TRPC6 but not TRPC5 knockdown (Fig. 5*H*).

Miro1 Mediates BDNF-induced Mitochondrial Motility Arrest—The above results demonstrate that TRPC3 and TRPC6 are essential for BDNF-induced intracellular Ca^{2+} elevation and mitochondrial stopping. We next investigated how the intracellular Ca^{2+} regulates mitochondrial motility in response to BDNF. Recently, several studies have demonstrated that Miro1, a mitochondrial outer membrane protein, acts as a Ca^{2+} sensor to regulate mitochondrial motility (13, 16). We hypothesized that Miro1 might also play a role in BDNF-regulated mitochondrial movement. To address this question, we transfected wild type (WT) or mutant Miro1 ($Miro1^{KK}$, EF-hand mutation resulting in the loss of Ca^{2+} binding) into cultured hippocampal neurons and analyzed the effects of BDNF on mitochondrial motility in the successfully transfected neurons. Consistent with previous reports, overexpression of either WT or mutant Miro1 caused a significant increase in the percentage of moving mitochondria (Fig. 6, *A–G*) (13). In neurons expressing the control vector or WT Miro1, BDNF reduced the percentage of anterograde-moving mitochondria by 41.1 ± 4.6% and 45.6 ± 5.0%, respectively (Fig. 6, *A–D* and *G*; quantification of retrograde-moving mitochondria was similar and is not shown). However, in neurons expressing $Miro1^{KK}$, BDNF lost the ability to cause mitochondria to stop (Fig. 6, *E–G*), which suggests that Miro1 mediates BDNF-induced mitochondrial stopping by binding with Ca^{2+}.

Two conflicting models have been proposed for Miro1-Ca^{2+}-mediated mitochondrial transport. The first proposes that upon Miro1 binding with Ca^{2+}, KIF5 is released from the Miro1-KIF5 complex on the mitochondrial surface, thereby halting mitochondrial movement (13). The other model proposes that elevated Ca^{2+} prevents the kinesin-Miro1 complex from binding to microtubules but leaves the complex on the mitochondrial surface, causing the arrest of mitochondrial movement (16). Because BDNF-regulated mitochondrial movement is also dependent on the Miro1-Ca^{2+} pathway, we investigated which model provided the best fit. We analyzed KIF5 and Miro1 protein levels in cytosolic and mitochondrial fractions from BDNF- or vehicle-treated neurons. The Western blot results revealed that treatment with BDNF for 15 min had no effect on the Miro1 and KIF5 protein levels in either the cytosolic or mitochondrial fractions (Fig. 6, *H* and *I*), suggesting that BDNF-induced mitochondrial stopping may be due to the dissociation of the KIF5-Miro1 complex from microtubules rather than to the dissociation of KIF5 from mitochondria.

To confirm the mechanism of the Miro1-dependent BDNF-induced mitochondrial motility arrest, the effects of Miro1/

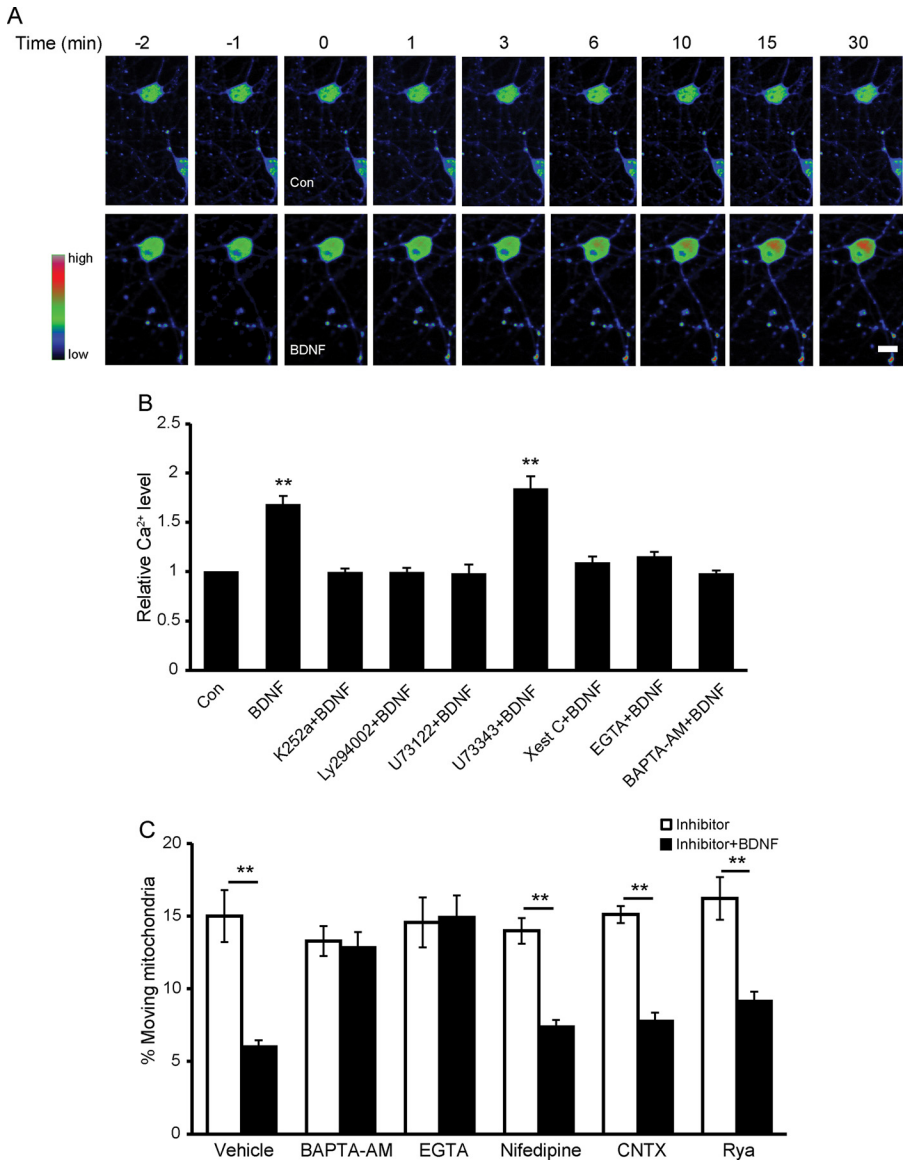

FIGURE 4. **BDNF-induced mitochondrial stopping is dependent on intracellular Ca^{2+} elevation.** *A,* representative pseudocolored images of neurons loaded with Fluo4-AM before and after the onset of BDNF or vehicle treatment (at time 0). *Scale bar,* 10 μm. *B,* normalized changes of intracellular Ca^{2+} levels in the absence or presence of BDNF for 15 min after pretreatment with various drugs. K252a, LY294002, U73122, and Xest C block BDNF-induced intracellular Ca^{2+} elevation. *C,* percentage of anterograde mitochondrial movement after a 15-min BDNF treatment in axons of control (*Con*) neurons ($n = 195$ mitochondria from seven axons), BAPTA-AM-pretreated neurons ($n = 254$ mitochondria from eight axons), EGTA-pretreated neurons ($n = 127$ mitochondria from seven axons), nifedipine-pretreated neurons ($n = 164$ mitochondria from seven axons), ω-conotoxin (*CNTX*)-pretreated neurons ($n = 154$ mitochondria from eight axons) or ryanodine (*Rya*)-pretreated neurons ($n = 117$ mitochondria from eight axons). Values are shown as the mean ± S.E. from at least three independent experiments, **, $p < 0.01$, Student's *t* test.

$Miro1^{KK}$ on intracellular Ca^{2+} concentration were examined. Overexpressing Miro1 or $Miro1^{KK}$ did not change the basal intracellular Ca^{2+} levels in somas. Moreover, in neurons expressing either Miro1 or $Miro1^{KK}$, BDNF could still cause intracellular Ca^{2+} increase to a degree similar to that in control neurons (Fig. 6*J*). The Ca^{2+} changes in axon terminals were similar to those in somas, and it is interestingly to note that BDNF induces higher calcium concentration at the axon terminals compared with that in the neighboring regions as shown in Fig. 6*K*. The surface TrkB levels in neurons expressing the empty vector, WT Miro1, and $Miro1^{KK}$ were also examined, and they did not show significant differences (Fig. 6, *L* and *M*). These results indicate that Miro1 and $Miro1^{KK}$ did not affect basal intracellular Ca^{2+} or BDNF-induced intracellular Ca^{2+} increase nor did they alter surface TrkB levels, suggesting that Miro1's effects on BDNF-regulated mitochondrial motility depend on its ability to bind Ca^{2+}.

BDNF-induced Increase of Mitochondria in the Stationary Pool Contributes to the Effect of BDNF on Neurotransmitter Release—Because mitochondria provide energy and calcium buffering functions that are important for neuronal activities such as synaptic transmission, we asked whether BDNF-induced arrest of mitochondrial movement played a role in BDNF-mediated synaptic transmission. We first examined the number and size of synaptic vesicles with SV2 immunostaining. BDNF treatment for 15 min did not change the number and size of synaptic vesicles compared with controls (Fig. 7, *A* and *B*). To determine whether BDNF-induced mitochondrial stopping led

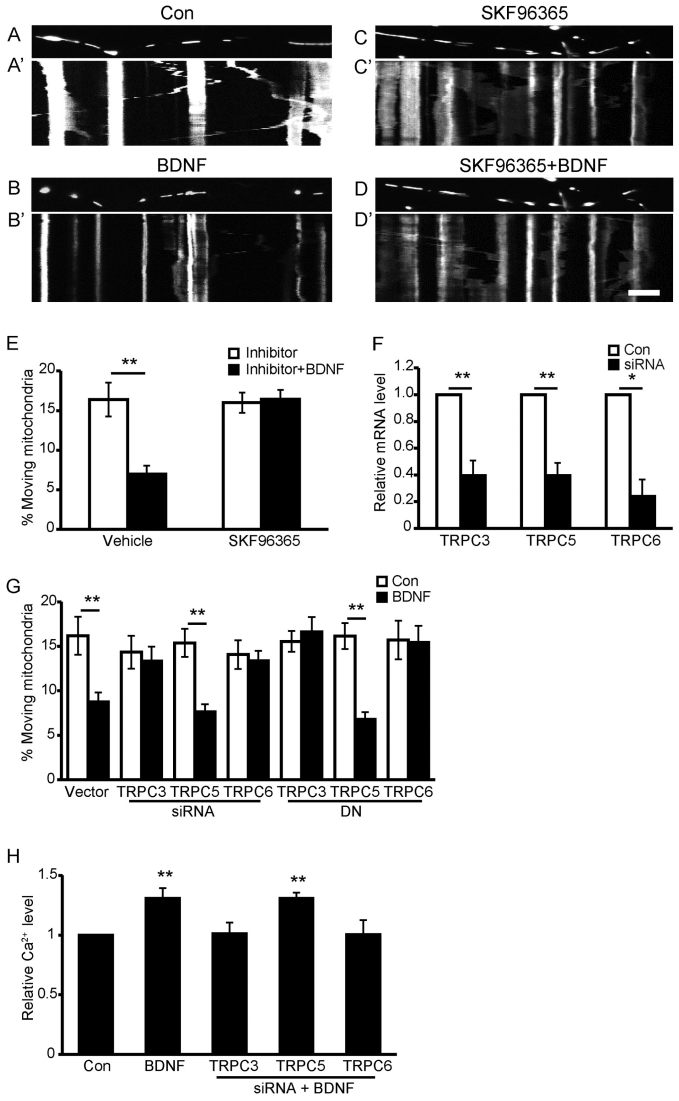

FIGURE 5. **Blockade of TRPC channels abolishes BDNF-induced mitochondrial stopping.** *A–D,* representative static images of mitochondria in axons before and after BDNF treatment in the presence or absence of SKF96365. *A′–D′*, representative kymographs of mitochondrial movement before and after BDNF treatment in the presence or absence of SKF96365. *Scale bar,* 10 μm; height, 5 min. *E,* percentage of anterograde-moving mitochondria before and after BDNF treatment in axons of control (*Con*) neurons ($n = 261$ mitochondria from 10 axons) or SKF96365-pretreated neurons ($n = 191$ mitochondria from 10 axons). *F,* down-regulation of TRPC3, TRPC5, and TRPC6 by siRNA was examined by real time PCR. *G,* percentage of anterograde-moving mitochondria before and after BDNF treatment in neurites of control neurons ($n = 125$ mitochondria from seven axons), TRPC3 siRNA-transfected neurons ($n = 122$ mitochondria from eight axons), TRPC6 siRNA-transfected neurons ($n = 137$ mitochondria from eight axons), TRPC5 siRNA-transfected neurons ($n = 217$ mitochondria from seven axons), DN-TRPC3-transfected neurons ($n = 178$ mitochondria from eight axons), DN-TRPC5-transfected neurons ($n = 171$ mitochondria from eight axons), or DN-TRPC6-transfected neurons ($n = 172$ mitochondria from seven axons). *H,* knocking down TRPC3 or TRPC6, but not TRPC5, prevents BDNF-induced intracellular Ca^{2+} elevation. Data are shown as the mean ± S.E. from three independent experiments, *, $p < 0.05$; **, $p < 0.01$, Student's *t* test.

to altered mitochondrial distribution, neurons expressing mitoDsRed2 were fixed after BDNF treatment for 15 min and then stained with the SV2 antibody. We analyzed mitochondrial localization at presynaptic sites. Axonal mitochondria localized within 1 μm from the SV2 puncta were regarded as colocalized with synaptic vesicles. After BDNF treatment, we observed a significantly increased percentage of mitochondria colocalized with SV2 puncta (Fig. 7, *C* and *D*), suggesting that BDNF treatment induces the accumulation of more mitochondria at presynaptic sites. Because Miro1 has been shown to mediate mitochondrial motility in response to BDNF, we asked whether BDNF-induced mitochondrial recruitment to presynaptic site depends on Miro1. We examined the effect of BDNF on the colocalization between mitochondria and SV2 in WT Miro1- or Miro1^{KK}-expressing neurons. As shown in Fig. 7*D*, WT Miro1 had no effect, but the Miro1^{KK} mutant blocked the increased colocalization between mitochondrial and SV2 triggered by BDNF. The above results indicate that BDNF could induce more mitochondrial docking at presynaptic sites and that this effect is dependent on Miro1.

We next investigated whether BDNF-induced Miro1-dependent mitochondrial presynaptic docking is associated with BDNF-modulated neurotransmitter release. Previous studies have reported that BDNF could rapidly enhance evoked synaptic transmission and spontaneous glutamate release (27). We first investigated whether WT Miro1 or Miro1^{KK} affects the basal number of active synaptic boutons, which is an indicator of the number of neurotransmitter release sites. FM 1-43 was used to label the presynaptic sites, as described under "Experimental Procedures." The number of active synaptic boutons per unit length in successfully transfected neurons was quantified. The neurons expressing WT Miro1 or Miro1^{KK} had similar numbers of active synaptic boutons (Fig. 8, *B* and *C*), suggesting that the Miro1 or mutant Miro1 does not affect the basal levels of active synaptic vesicles. We next examined whether Miro1 is involved in BDNF-enhanced neurotransmitter release. Consistent with a previous report, BDNF increased K^+-evoked neurotransmitter release in control neurons (Fig. 8, *D* and *E*) (35). This effect was blocked by the Miro1^{KK} mutant but not by WT Miro1 (Fig. 8*E*), suggesting that Miro1's activity as a Ca^{2+} sensor mediates BDNF-enhanced neurotransmitter release. Together, these data indicate that Miro1 mediates BDNF-induced mitochondrial presynaptic accumulation and BDNF-enhanced synaptic transmission.

DISCUSSION

This study shows that BDNF increased the proportion of stationary mitochondria, which is dependent on the elevation of intracellular Ca^{2+} induced by the activation of PI3K and PLCγ-IP_3 pathways and TRPC3/6 channels. Miro1, functioning as a Ca^{2+} sensor, dissociates KIF5 from microtubules, resulting in more mitochondria recruited into presynaptic sites, and thereby enhancing synaptic transmission.

Our studies provide several insights into the molecular mechanisms and significance of BDNF-regulated mitochondrial motility. To our knowledge, this is the first report to show that BDNF specifically regulates mitochondrial motility. We showed that BDNF-induced mitochondrial stopping is dependent on TrkB receptor tyrosine kinase activity and its downstream PI3K and PLCγ signaling pathways (Figs. 3 and 4). Previously, Chada and Hollenbeck (8, 36) demonstrated that focal stimulation with NGF-coated beads causes a local accumulation of mitochondria in axons and that this is dependent on the activation of PI3K. Given the high structural similarity

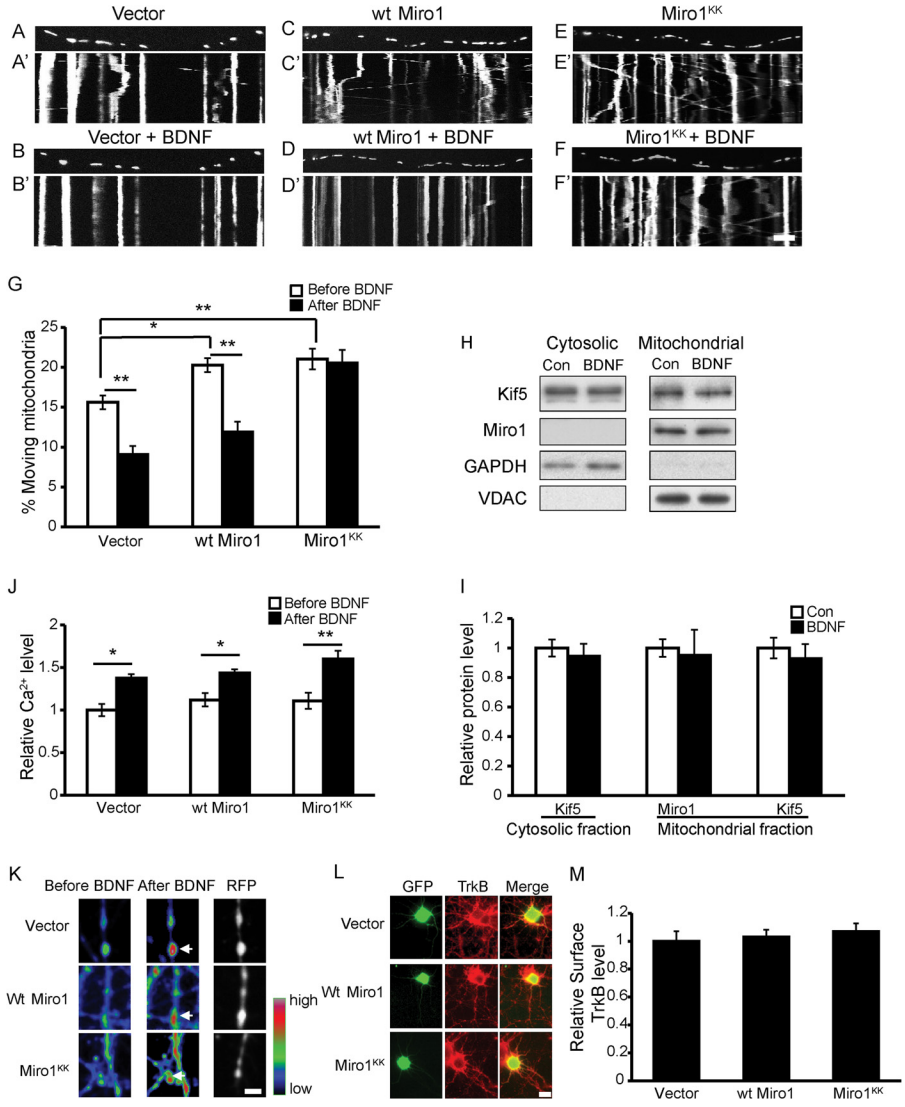

FIGURE 6. **Miro1 is required for BDNF-induced mitochondria stopping.** *A–F,* representative static images of mitochondria in axons of neurons expressing the control vector (*A* and *B*), WT Miro1 (*C* and *D*), or Miro1^{KK} (*E* and *F*) before and after BDNF treatment. *A′–F′,* representative kymographs of moving mitochondria in control (*A′* and *B′*), WT Miro1 (*C′* and *D′*), and Miro1^{KK} (*E′* and *F′*) neurons before and after BDNF treatment. *Scale bar,* 10 μm; height, 5 min. *G,* percentage of anterograde-moving mitochondria before and after BDNF treatment in axons of empty vector-transfected neurons ($n = 125$ mitochondria from 7 axons), WT Miro1-transfected neurons ($n = 180$ mitochondria from nine axons), and Miro1^{KK}-transfected neurons ($n = 172$ mitochondria from nine axons). *H,* representative Western blot images of Miro1 and KIF5 in cytosolic and mitochondrial fractions after BDNF treatment for 15 min. *I,* quantification of data as in *H* from four independent experiments. *J,* overexpressing WT Miro1 or Miro1^{KK} did not affect basal intracellular Ca^{2+} levels or BDNF-induced Ca^{2+} up-regulation in somas. *K,* representative pseudocolored images of axonal terminals of neurons with empty vector, WT Miro1, or Miro1^{KK} overexpression loaded with Fluo4-AM before and after BDNF treatment. Red fluorescent protein (*RFP*) was used to indicate the successfully transfected neuron terminals. *Arrows* indicate the Ca^{2+} changes at axon terminals. *Scale bar,* 5 μm. *L,* representative images of surface TrkB levels in neurons with empty vector, WT Miro1, or Miro1^{KK} expression; quantification results are shown in *M*, *scale bar,* 20 μm. Values are shown as the mean ± S.E. from three independent experiments, *, $p < 0.05$; **, $p < 0.01$, one-way analysis of variance followed by post hoc tests or Student's *t* test. *Con*, control.

between NGF and BDNF, it is likely that neurotrophic factors share common signaling pathways to regulate mitochondrial trafficking.

In neurons, the elevation of intracellular Ca^{2+} through voltage-dependent Ca^{2+} channels or NMDA receptors has been reported to arrest microtubule-based mitochondrial movement (11, 12, 37). We showed that, following activation of PI3K and PLCγ, the intracellular Ca^{2+} concentration was significantly increased by a mechanism dependent on IP_3 and TRPC3/6 channels. Indeed, it has been reported that the activation of PLCγ-IP_3 by BDNF leads to Ca^{2+} release from internal stores, which then activates store-operated TRPC channels and allows a sustained extracellular Ca^{2+} influx (30). PI3K has also been reported to induce accumulation of phosphatidylinositol 3,4,5-trisphosphate as a signaling node to asymmetric activation of Akt, leading to potentiation of TRPC channels in the membrane and allowing the influx of Ca^{2+} (38). It is noteworthy that both PI3K and PLCγ are required for BDNF-induced Ca^{2+} elevation and mitochondrial stopping; blocking either of the pathways could abolish BDNF's effects. Similarly, BDNF-induced Ca^{2+}-dependent growth cone turning requires both PI3K and PLCγ activation (19). How these two molecules or pathways jointly regulate BDNF's function requires further investigation.

TRPC channels are a family of nonselective Ca^{2+}-permeable cation channels. They can form functional heteromeric or

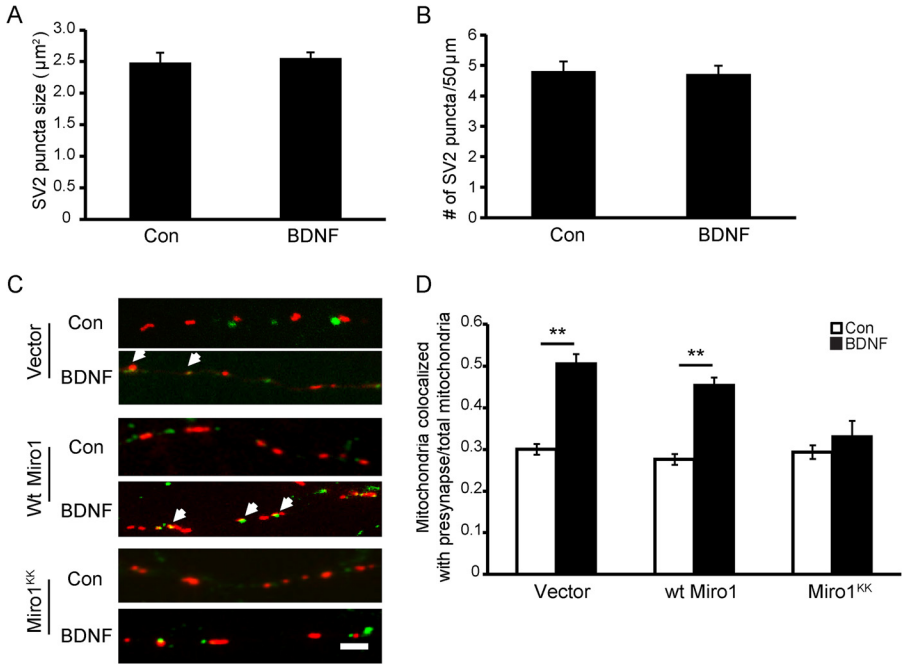

FIGURE 7. **BDNF induces mitochondria recruited to presynaptic site dependent on Miro1 binding with Ca^{2+}.** *A* and *B,* transient application of BDNF had no effect on the size and density of SV2-labeled puncta. *C,* representative images of presynaptic mitochondria (in *red*) and SV2-labeled puncta (in *green*) in neuronal axons with empty vector, WT Miro1, and $Miro1^{KK}$ expression before and after BDNF treatment. The *arrows* indicate the colocalization between mitochondria and SV2. *Scale bar,* 5 μm. *D,* colocalization index (mitochondria colocalized with SV2/total mitochondria) in neurons expressing empty vector, WT Miro1, or $Miro1^{KK}$ before and after BDNF treatment. Values are shown as the mean ± S.E. from three independent experiments, **, $p < 0.01$, Student's *t* test. *Con,* control.

homomeric channels (39, 40) and participate in diverse neuronal functions, including cell survival, spine formation, neurite growth, and growth cone turning (19, 30, 32, 33). TRPC3 and TRPC6 channels have been demonstrated to localize to synapses (31, 41), and TRPC3- and TRPC6-mediated Ca^{2+} influx is critical for BDNF-induced growth cone guidance and survival of cerebellar granule cells (19, 32). In our study, we demonstrate that TRPC3 and TRPC6, but not TRPC5, also play critical roles in BDNF-regulated mitochondrial docking (Fig. 5). It has been speculated that by allowing different patterns of Ca^{2+} influx, diverse TRPC channels may perform distinct regulatory functions in neurons. Indeed, a recent study demonstrated that TRPC5-mediated Ca^{2+} elevation activates CaMKIIα, whereas TRPC6-mediated Ca^{2+} elevation activates CaMKIV, resulting in inhibition and promotion of neuronal dendritic growth, respectively (42). In our experiments, it is likely that at presynaptic sites TRPC3 forms heteromers with TRPC6 and is activated by BDNF, allowing Ca^{2+} influx and resulting in higher intracellular Ca^{2+} at the synaptic sites, which leads to more mitochondrial docking at synaptic sites regardless of anterograde or retrograde movement of mitochondria. Interestingly, Feng *et al.* (43) recently reported that TRPC3 localizes not only to plasma membrane but also to the inner mitochondrial membrane and that it contributes to mitochondrial Ca^{2+} uptake. One study has suggested mitochondrial matrix Ca^{2+} content to be an intrinsic signal for modulating mitochondrial motility in neurons (44). Thus, we speculate that mitochondrial TRPC3 channels may also contribute to BDNF-mediated mitochondrial motility by mediating mitochondrial Ca^{2+} levels.

Miro1 is required for BDNF-induced mitochondrial docking at synaptic sites. Miro1 is a mitochondrial outer membrane protein with two EF-hand domains, which bind Ca^{2+}, and several recent studies have demonstrated that KIF5, Miro1, and TRAK/Milton form a complex that mediates Ca^{2+}-dependent regulation of mitochondrial motility (13, 16, 45). We demonstrated that Miro1, in its role as a Ca^{2+} sensor, regulates BDNF-induced mitochondria recruitment to presynaptic sites. A study using *Drosophila* has similarly demonstrated that Miro is required for controlling the anterograde transport of mitochondria and their proper distribution within nerve terminals (14). The fact that BDNF-enhanced synaptic transmission could be blocked by mutant Miro1 may be due to the lack of synaptic mitochondria. Two different models of Miro1 regulation of mitochondrial motility have been proposed. One model suggests that elevated Ca^{2+} causes dissociation of KIF5 from the Miro1-motor complex (13); the other suggests that the KIF5-Miro1 complex dissociates from microtubules in response to elevated Ca^{2+} (16). Our data favor the model that the KIF5-Miro1 complex dissociates from microtubules upon BDNF treatment, thus causing reduced mitochondrial motility.

It is worth noting that an intact actin cytoskeleton is required for mitochondrial docking induced by NGF (8). We speculate that in addition to Miro1-mediated microtubule-based movement, actin-based mitochondrial movement is also involved in BDNF-induced mitochondrial docking, and myosin motors might be involved in regulating the interaction between mitochondria and actin at synaptic sites upon BDNF treatment.

Finally, our data suggest that the recruitment of more mitochondria for docking at presynaptic sites contributes to BDNF-enhanced neurotransmitter release. BDNF-enhanced neurotransmitter release has been previously reported (46, 47), and it has been demonstrated that synapsin is phosphorylated by

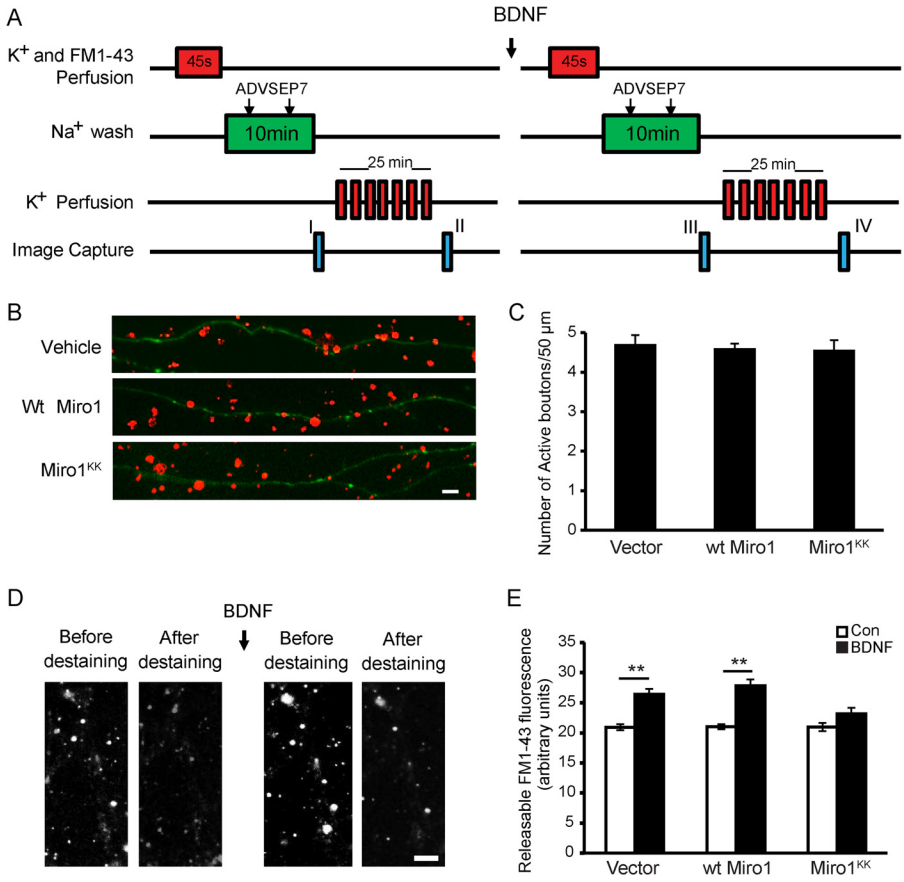

FIGURE 8. **Requirement of Miro1 for BDNF-enhanced neurotransmitter release.** *A,* experimental protocol for FM 1-43 staining and destaining of synaptic vesicles. ADVASEP-7 was used for enhanced removal of the dye from the external medium. Two images were taken after staining (*I*) and destaining (*II*), respectively. The difference in the number of FM 1-43-stained boutons between images (*I* and *II*) indicates the active synaptic vesicles. To study the effects of BDNF on neurotransmitter release, BDNF was added as shown. Releasable FM 1-43 fluorescence intensity (differences between images *I* and *II* and images *III* and *IV*) was measured. The differences in the changes of fluorescence intensity in neurons transfected with empty vector, WT Miro1, or Miro1^{KK} before and after BDNF treatment were quantitated. *B,* representative images of FM 1-43 staining of synaptic boutons in neurons transfected with empty vector, WT Miro1, or Miro1^{KK}. *Green* indicates GFP-expressing axons, and *red* indicates FM 1-43 staining. *Scale bar,* 5 μm. *C,* quantification of active FM 1-43 stained boutons from three independent experiments. *D,* representative images from staining and destaining with FM 1-43 before and after BDNF application. *Scale bar,* 10 μm. *E,* quantification of releasable FM 1-43 fluorescence intensity in neurons expressing empty vector, WT Miro1, and Miro1^{KK}. Values are shown as the mean $\pm$ S.E. from three independent experiments, **, $p < 0.01$, one-way analysis of variance followed by post hoc tests or Student's *t* test.

MAPK and that Myo6 and GIPC1 are associated with BDNF-enhanced synaptic transmission (27, 48). Recently, Amaral and Pozzo-Miller (49) reported that BDNF could enhance spontaneous quantal transmitter release through a Ca^{2+}-dependent mechanism. We provide evidence that Miro1's ability to bind Ca^{2+} is required for BDNF-enhanced neurotransmitter release. This suggests that Miro1 is one of the downstream effectors of calcium, regulating BDNF-enhanced synaptic transmission most likely via its mediation of mitochondrial docking at presynaptic sites. Such a mechanism is consistent with previous findings that mutant Miro reduces the population of presynaptic mitochondria and causes impaired neurotransmitter release (14). Several studies have demonstrated that mitochondria are required at synapses to help maintain neurotransmission by buffering Ca^{2+} (1, 14). It has also been reported that BDNF-enhanced neurotransmitter release is due to increases in the number of vesicles docked at the active zone of individual synapses (50), which is partly dependent on mitochondrial ATP production (51). One recent study has shown that presynaptic mitochondria are essential determinants of synaptic vesicle exocytosis, primarily via ATP synthesis (52). In the case of BDNF-enhanced neurotransmitter release, although an overall increase in ATP production was not observed (Fig. 2*C*), we speculate that there is an increase in ATP production at presynaptic sites due to more mitochondria localized at the area, thus facilitating synaptic transmission.

In conclusion, our study reveals that BDNF could increase the stationary mitochondrial pool in axons and that this is mediated by elevation of intracellular Ca^{2+}. Furthermore, the BDNF-induced mitochondrial motility arrest causes more mitochondria to be recruited at presynaptic sites, which plays an important role in BDNF enhanced neurotransmitter release. These findings might provide insights not only into the mechanistic link between BDNF-dependent mitochondrial motility and BDNF-mediated synaptic transmission but also more generally into the fields of mitochondrial transport and neurotransmission.

REFERENCES

1. Billups, B., and Forsythe, I. D. (2002) Presynaptic mitochondrial calcium sequestration influences transmission at mammalian central synapses. *J. Neurosci.* **22,** 5840–5847
2. Li, Z., Okamoto, K., Hayashi, Y., and Sheng, M. (2004) The importance of dendritic mitochondria in the morphogenesis and plasticity of spines and

synapses. *Cell* **119,** 873–887
3. Hirokawa, N., Sato-Yoshitake, R., Kobayashi, N., Pfister, K. K., Bloom, G. S., and Brady, S. T. (1991) Kinesin associates with anterogradely transported membranous organelles *in vivo*. *J. Cell Biol.* **114,** 295–302
4. Kanai, Y., Okada, Y., Tanaka, Y., Harada, A., Terada, S., and Hirokawa, N. (2000) KIF5C, a novel neuronal kinesin enriched in motor neurons. *J. Neurosci.* **20,** 6374–6384
5. Tanaka, Y., Kanai, Y., Okada, Y., Nonaka, S., Takeda, S., Harada, A., and Hirokawa, N. (1998) Targeted disruption of mouse conventional kinesin heavy chain, kif5B, results in abnormal perinuclear clustering of mitochondria. *Cell* **93,** 1147–1158
6. Nangaku, M., Sato-Yoshitake, R., Okada, Y., Noda, Y., Takemura, R., Yamazaki, H., and Hirokawa, N. (1994) KIF1B, a novel microtubule plus end-directed monomeric motor protein for transport of mitochondria. *Cell* **79,** 1209–1220
7. Tanaka, K., Sugiura, Y., Ichishita, R., Mihara, K., and Oka, T. (2011) KLP6: a newly identified kinesin that regulates the morphology and transport of mitochondria in neuronal cells. *J. Cell Sci.* **124,** 2457–2465
8. Chada, S. R., and Hollenbeck, P. J. (2004) Nerve growth factor signaling regulates motility and docking of axonal mitochondria. *Curr. Biol.* **14,** 1272–1276
9. Chen, S., Owens, G. C., Crossin, K. L., and Edelman, D. B. (2007) Serotonin stimulates mitochondrial transport in hippocampal neurons. *Mol. Cell. Neurosci.* **36,** 472–483
10. Chen, S., Owens, G. C., and Edelman, D. B. (2008) Dopamine inhibits mitochondrial motility in hippocampal neurons. *PLoS One* **3,** e2804
11. Rintoul, G. L., Filiano, A. J., Brocard, J. B., Kress, G. J., and Reynolds, I. J. (2003) Glutamate decreases mitochondrial size and movement in primary forebrain neurons. *J. Neurosci.* **23,** 7881–7888
12. Yi, M., Weaver, D., and Hajnóczky, G. (2004) Control of mitochondrial motility and distribution by the calcium signal: a homeostatic circuit. *J. Cell Biol.* **167,** 661–672
13. Macaskill, A. F., Rinholm, J. E., Twelvetrees, A. E., Arancibia-Carcamo, I. L., Muir, J., Fransson, A., Aspenstrom, P., Attwell, D., and Kittler, J. T. (2009) Miro1 is a calcium sensor for glutamate receptor-dependent localization of mitochondria at synapses. *Neuron* **61,** 541–555
14. Guo, X., Macleod, G. T., Wellington, A., Hu, F., Panchumarthi, S., Schoenfield, M., Marin, L., Charlton, M. P., Atwood, H. L., and Zinsmaier, K. E. (2005) The GTPase dMiro is required for axonal transport of mitochondria to *Drosophila* synapses. *Neuron* **47,** 379–393
15. Glater, E. E., Megeath, L. J., Stowers, R. S., and Schwarz, T. L. (2006) Axonal transport of mitochondria requires milton to recruit kinesin heavy chain and is light chain independent. *J. Cell Biol.* **173,** 545–557
16. Wang, X., and Schwarz, T. L. (2009) The mechanism of Ca^{2+}-dependent regulation of kinesin-mediated mitochondrial motility. *Cell* **136,** 163–174
17. Numakawa, T., Suzuki, S., Kumamaru, E., Adachi, N., Richards, M., and Kunugi, H. (2010) BDNF function and intracellular signaling in neurons. *Histol. Histopathol.* **25,** 237–258
18. Markham, A., Cameron, I., Franklin, P., and Spedding, M. (2004) BDNF increases rat brain mitochondrial respiratory coupling at complex I, but not complex II. *Eur. J. Neurosci.* **20,** 1189–1196
19. Li, Y., Jia, Y. C., Cui, K., Li, N., Zheng, Z. Y., Wang, Y. Z., and Yuan, X. B. (2005) Essential role of TRPC channels in the guidance of nerve growth cones by brain-derived neurotrophic factor. *Nature* **434,** 894–898
20. Graham, S., Ding, M., Ding, Y., Sours-Brothers, S., Luchowski, R., Gryczynski, Z., Yorio, T., Ma, H., and Ma, R. (2010) Canonical transient receptor potential 6 (TRPC6), a redox-regulated cation channel. *J. Biol. Chem.* **285,** 23466–23476
21. Shin, H. Y., Hong, Y. H., Jang, S. S., Chae, H. G., Paek, S. L., Moon, H. E., Kim, D. G., Kim, J., Paek, S. H., and Kim, S. J. (2010) A role of canonical transient receptor potential 5 channel in neuronal differentiation from A2B5 neural progenitor cells. *PLoS One* **5,** e10359
22. Zhao, L., Sheng, A. L., Huang, S. H., Yin, Y. X., Chen, B., Li, X. Z., Zhang, Y., and Chen, Z. Y. (2009) Mechanism underlying activity-dependent insertion of TrkB into the neuronal surface. *J. Cell Sci.* **122,** 3123–3136
23. Yoshii, A., and Constantine-Paton, M. (2007) BDNF induces transport of PSD-95 to dendrites through PI3K-AKT signaling after NMDA receptor activation. *Nat. Neurosci.* **10,** 702–711
24. Cheung, Z. H., Chin, W. H., Chen, Y., Ng, Y. P., and Ip, N. Y. (2007) Cdk5 is involved in BDNF-stimulated dendritic growth in hippocampal neurons. *PLoS Biol.* **5,** e63
25. Ma, L., Zablow, L., Kandel, E. R., and Siegelbaum, S. A. (1999) Cyclic AMP induces functional presynaptic boutons in hippocampal CA3-CA1 neuronal cultures. *Nat. Neurosci.* **2,** 24–30
26. Ninan, I., and Arancio, O. (2004) Presynaptic CaMKII is necessary for synaptic plasticity in cultured hippocampal neurons. *Neuron* **42,** 129–141
27. Yano, H., Ninan, I., Zhang, H., Milner, T. A., Arancio, O., and Chao, M. V. (2006) BDNF-mediated neurotransmission relies upon a myosin VI motor complex. *Nat. Neurosci.* **9,** 1009–1018
28. Markham, A., Cameron, I., Bains, R., Franklin, P., Kiss, J. P., Schwendimann, L., Gressens, P., and Spedding, M. (2012) Brain-derived neurotrophic factor-mediated effects on mitochondrial respiratory coupling and neuroprotection share the same molecular signalling pathways. *Eur. J. Neurosci.* **35,** 366–374
29. Walsh, B., Tonkonogi, M., Söderlund, K., Hultman, E., Saks, V., and Sahlin, K. (2001) The role of phosphorylcreatine and creatine in the regulation of mitochondrial respiration in human skeletal muscle. *J. Physiol.* **537,** 971–978
30. Amaral, M. D., and Pozzo-Miller, L. (2007) TRPC3 channels are necessary for brain-derived neurotrophic factor to activate a nonselective cationic current and to induce dendritic spine formation. *J. Neurosci.* **27,** 5179–5189
31. Li, H. S., Xu, X. Z., and Montell, C. (1999) Activation of a TRPC3-dependent cation current through the neurotrophin BDNF. *Neuron* **24,** 261–273
32. Jia, Y., Zhou, J., Tai, Y., and Wang, Y. (2007) TRPC channels promote cerebellar granule neuron survival. *Nat. Neurosci.* **10,** 559–567
33. Greka, A., Navarro, B., Oancea, E., Duggan, A., and Clapham, D. E. (2003) TRPC5 is a regulator of hippocampal neurite length and growth cone morphology. *Nat. Neurosci.* **6,** 837–845
34. Bezzerides, V. J., Ramsey, I. S., Kotecha, S., Greka, A., and Clapham, D. E. (2004) Rapid vesicular translocation and insertion of TRP channels. *Nat. Cell Biol.* **6,** 709–720
35. Bradley, J., and Sporns, O. (1999) BDNF-dependent enhancement of exocytosis in cultured cortical neurons requires translation but not transcription. *Brain Res.* **815,** 140–149
36. Chada, S. R., and Hollenbeck, P. J. (2003) Mitochondrial movement and positioning in axons: the role of growth factor signaling. *J. Exp. Biol.* **206,** 1985–1992
37. Chang, D. T., Honick, A. S., and Reynolds, I. J. (2006) Mitochondrial trafficking to synapses in cultured primary cortical neurons. *J. Neurosci.* **26,** 7035–7045
38. Henle, S. J., Wang, G., Liang, E., Wu, M., Poo, M. M., and Henley, J. R. (2011) Asymmetric $PI(3,4,5)P_3$ and Akt signaling mediates chemotaxis of axonal growth cones. *J. Neurosci.* **31,** 7016–7027
39. Hofmann, T., Schaefer, M., Schultz, G., and Gudermann, T. (2002) Subunit composition of mammalian transient receptor potential channels in living cells. *Proc. Natl. Acad. Sci. U.S.A.* **99,** 7461–7466
40. Goel, M., Sinkins, W. G., and Schilling, W. P. (2002) Selective association of TRPC channel subunits in rat brain synaptosomes. *J. Biol. Chem.* **277,** 48303–48310
41. Zhou, J., Du, W., Zhou, K., Tai, Y., Yao, H., Jia, Y., Ding, Y., and Wang, Y. (2008) Critical role of TRPC6 channels in the formation of excitatory synapses. *Nat. Neurosci.* **11,** 741–743
42. He, Z., Jia, C., Feng, S., Zhou, K., Tai, Y., Bai, X., and Wang, Y. (2012) TRPC5 channel is the mediator of neurotrophin-3 in regulating dendritic growth via CaMKIIα in rat hippocampal neurons. *J. Neurosci.* **32,** 9383–9395
43. Feng, S., Li, H., Tai, Y., Huang, J., Su, Y., Abramowitz, J., Zhu, M. X., Birnbaumer, L., and Wang, Y. (2013) Canonical transient receptor potential 3 channels regulate mitochondrial calcium uptake. *Proc. Natl. Acad. Sci. U.S.A.* **110,** 11011–11016
44. Chang, K. T., Niescier, R. F., and Min, K. T. (2011) Mitochondrial matrix Ca^{2+} as an intrinsic signal regulating mitochondrial motility in axons. *Proc. Natl. Acad. Sci. U.S.A.* **108,** 15456–15461
45. Saotome, M., Safiulina, D., Szabadkai, G., Das, S., Fransson, A., Aspen-

strom, P., Rizzuto, R., and Hajnóczky, G. (2008) Bidirectional Ca^{2+}-dependent control of mitochondrial dynamics by the Miro GTPase. *Proc. Natl. Acad. Sci. U.S.A.* **105,** 20728–20733
46. Ji, Y., Lu, Y., Yang, F., Shen, W., Tang, T. T., Feng, L., Duan, S., and Lu, B. (2010) Acute and gradual increases in BDNF concentration elicit distinct signaling and functions in neurons. *Nat. Neurosci.* **13,** 302–309
47. Kang, H., and Schuman, E. M. (1995) Long-lasting neurotrophin-induced enhancement of synaptic transmission in the adult hippocampus. *Science* **267,** 1658–1662
48. Jovanovic, J. N., Czernik, A. J., Fienberg, A. A., Greengard, P., and Sihra, T. S. (2000) Synapsins as mediators of BDNF-enhanced neurotransmitter release. *Nat. Neurosci.* **3,** 323–329
49. Amaral, M. D., and Pozzo-Miller, L. Intracellular Ca^{2+} stores and Ca^{2+} influx are both required for BDNF to rapidly increase quantal vesicular transmitter release. *Neural Plasticity* 2012:203536,2012
50. Tyler, W. J., and Pozzo-Miller, L. D. (2001) BDNF enhances quantal neurotransmitter release and increases the number of docked vesicles at the active zones of hippocampal excitatory synapses. *J. Neurosci.* **21,** 4249–4258
51. Verstreken, P., Ly, C. V., Venken, K. J., Koh, T. W., Zhou, Y., and Bellen, H. J. (2005) Synaptic mitochondria are critical for mobilization of reserve pool vesicles at *Drosophila* neuromuscular junctions. *Neuron* **47,** 365–378
52. Ivannikov, M. V., Sugimori, M., and Llinás, R. R. (2013) Synaptic vesicle exocytosis in hippocampal synaptosomes correlates directly with total mitochondrial volume. *J. Mol. Neurosci.* **49,** 223–230